Folding Kinetics of the S100A11 Protein Dimer Studied by Time-Resolved Electrospray Mass Spectrometry and Pulsed Hydrogen−Deuterium Exchange†

Jingxi Pan,‡ Anne C. Rintala-Dempsey,§ Yu Li,‡ Gary S. Shaw,‡,§ and Lars Konermann*,‡,§

Department of Chemistry and Department of Biochemistry, The University of Western Ontario, London, Ontario N6A 5B7, Canada

Received November 17, 2005; Revised Manuscript Received January 7, 2006

ABSTRACT: This study reports the application of electrospray ionization (ESI) mass spectrometry (MS) with on-line rapid mixing for millisecond time-resolved studies of the refolding and assembly of a dimeric protein complex. Acid denaturation of S100A11 disrupts the native homodimeric protein structure. Circular dichroism and HSQC nuclear magnetic resonance measurements reveal that the monomeric subunits unfold to a moderate degree but retain a significant helicity and some tertiary structural elements. Following a rapid change in solution conditions to a slightly basic pH, the native protein reassembles with an effective rate constant of 6 s^{-1}. The ESI charge state distributions measured during the reaction suggest the presence of three kinetic species, namely, a relatively unfolded monomer (M_U), a more tightly folded monomeric reaction intermediate (M_F), and dimeric S100A11. These three forms exhibit distinct calcium binding properties, with very low metal loading levels for M_U, up to two calcium ions for M_F, and up to four for the dimer. Surprisingly, on-line pulsed hydrogen−deuterium exchange (HDX) reveals that each of the monomeric forms of the protein comprises two subspecies that can be distinguished on the basis of their isotope exchange levels. As the reaction proceeds, the more extensively labeled species are depleted. The exponential nature of the measured intensity−time profiles implies that the rate-determining step of the overall process is a unimolecular event. The kinetics are consistent with a sequential folding and assembly mechanism involving two increasingly nativelike monomeric intermediates en route to the native S100A11 dimer.

The mechanisms by which denatured proteins spontaneously fold into their native structures have been a focal point of research for several decades (*1*). In recent years, many fundamental principles governing the folding of single-chain polypeptides have been uncovered (*2*−*5*). In contrast, surprisingly little effort has been directed toward the assembly of multisubunit structures from their unfolded constituents. The formation of quaternary protein assemblies adds another layer of complexity to the protein folding problem because folding and binding can be closely intertwined (*6*−*15*). Kinetic studies on protein association processes are challenging since spectroscopic signals such as fluorescence, circular dichroism, and even NMR[1] methods cannot readily distinguish unimolecular events from those that are linked to the formation of intermolecular contacts. Light and X-ray scattering methods exhibit relatively poor selectivity. Size fractionation and chemical cross-linking approaches have a limited kinetic resolution (*16*). The frequent occurrence of off-pathway aggregation is another general concern for studies on coupled folding−assembly processes (*8*).

Electrospray ionization (ESI) mass spectrometry (MS) offers an interesting alternative to the more traditional approaches for monitoring protein−ligand and protein−protein interactions (*17*). Intact protein assemblies can be transferred into the gas phase as multiply protonated entities so that binding stoichiometries can be deduced directly from the mass of the observed ions (*18*−*20*). In addition, the ESI charge state distribution provides a highly sensitive probe of the overall conformational properties of proteins in solution. Compact protein structures give rise to relatively low protonation states. Solution-phase unfolding greatly increases the extent of protonation, thereby shifting the overall peak distribution to higher charge states (*18*, *21*, *22*). Thus, ESI-MS provides a tool for monitoring protein conformational changes that are associated with the formation or disruption of intermolecular noncovalent interactions (*17*, *23*, *24*). The coupling of continuous-flow rapid mixing devices to the ESI source of a mass spectrometer allows protein folding and unfolding kinetics to be monitored with a temporal resolution of a few milliseconds ("time-resolved" ESI-MS) (*25*, *26*). Incorporation of an on-line pulsed hydrogen−deuterium exchange (HDX) step provides structural insights that are complementary to the information obtained from the ESI charge state distribution (*27*). Time-resolved ESI-MS has previously been used in studying folding processes that are coupled to the binding of prosthetic groups (*28*), as well as

† This work was supported by the Natural Sciences and Engineering Research Council of Canada (NSERC), the Canadian Institutes of Health Research (CIHR), the Canada Foundation for Innovation (CFI), the Province of Ontario, and the Canada Research Chairs Program.

* To whom correspondence should be addressed. Telephone: (519) 661-2111, ext. 86313. Fax: (519) 661-3022. E-mail: konerman@uwo.ca.

‡ Department of Chemistry.

§ Department of Biochemistry.

[1] Abbreviations: ESI, electrospray ionization; HDX, hydrogen−deuterium exchange; HSQC, heteronuclear single-quantum correlation; MS, mass spectrometry; NMR, nuclear magnetic resonance.

10.1021/bi052349a CCC: $33.50
Published on Web 02/07/2006

in monitoring the unfolding and subunit disassembly of multiprotein systems (*25*, *26*). This work demonstrates for the first time the feasibility of using this approach for kinetic studies of the formation of native protein complexes, starting from their denatured, monomeric constituents.

The S100 protein family is a highly conserved group of EF-hand calcium-binding proteins with molecular masses ranging from 10 to 12 kDa. Approximately 20 different S100 proteins have been identified with seemingly distinct functions and tissue distributions (*29*). They are involved in the regulation of protein phosphorylation, enzyme activity, cytoskeleton dynamics, and tumor suppression (*30*, *31*). These diverse functions are related to the proteins' ability to undergo calcium-induced conformational changes that allow them to interact with specific target polypeptide chains.

Like most other members of the S100 family, S100A11 (also termed S100C or calgizzarin) is a largely α-helical protein that forms a symmetric, homodimeric quaternary structure in both its apo- and calcium-loaded form. The four helices in each of the monomers are arranged into two helix−loop−helix calcium binding motifs, for a total of four binding sites per S100A11 dimer. The dissociation constant of this protein−protein complex has not been reported in the literature. However, binding studies on a number of similar S100 proteins have resulted in K_d values of ∼2 μM for the apo forms, whereas 10-fold higher affinities were found in the presence of calcium (*32*). Recently, a NMR structure of apo-S100A11 has become available (*33*), in addition to an earlier X-ray structure of the calcium-loaded dimer bound to two annexin I peptides (*30*). Comparison of these two structures reveals that calcium-mediated binding to the target peptide is associated with relatively subtle conformational alterations, reminiscent of those observed for troponin C (*34*), but quite different from the dramatic structural changes seen for other EF-hand proteins such as calmodulin (*35*). Dimeric apo-S100A11 forms a tightly folded globular structure, with short helices II (II′) and III (III′) in a near-antiparallel orientation. Upon binding to calcium and to the target peptide, helix III (III′) is tilted by roughly 30° (*33*).

In this study, the folding and dimerization of S100A11 are monitored by time-resolved ESI-MS in conjunction with on-line pulsed HDX. The formation of the native protein dimer occurs on the time scale of roughly 1 s. The overall process exhibits a surprising degree of complexity; it involves a number of monomeric intermediates that can be distinguished on the basis of their ESI charge state distributions, their calcium binding properties, and their HDX characteristics. The rate-determining step appears to be a conformational change at the monomer level. Overall, the data presented in this work clearly demonstrate the utility of time-resolved ESI-MS for studies on rapid biomolecular recognition and assembly processes.

EXPERIMENTAL PROCEDURES

Chemicals. Deuterium oxide (Cambridge Isotope Laboratories, Andover, MA), acetic acid (Caledon Laboratories, Georgetown, ON), ammonium acetate and ammonium hydroxide (Fisher Scientific, Nepean, ON), and calcium chloride ($CaCl_2$, Aldrich) were used as received. Solution pH and pD values were measured using an accumet pH meter (Fisher). Reported pD values were corrected for isotope effects on the basis of the relation pD = pH meter reading + 0.4 (*36*).

Sample Preparation. Recombinant rabbit S100A11 was expressed and purified as described previously (*33*, *37*). To avoid potential complications associated with intermolecular disulfide bridging (*30*), all experiments were carried out on the Cys9Ser variant of the protein. The molecular mass expected for the monomer based on its amino acid sequence is 11 281 Da. However, because all the protein samples used for this study were originally designed to be used in NMR experiments, they were carried out on uniformly ^{15}N labeled S100A11 with a molecular mass of 11 417 Da. The monomeric protein has a total of 182 exchangeable hydrogens, 96 of which are in backbone amide groups, 83 on side chains, and 3 on the termini.

Circular Dichroism Spectroscopy. CD spectra were recorded on a Jasco (Easton, MD) J-810 spectropolarimeter using a 1 mm path length cuvette and a protein concentration of 20 μM (based on monomeric S100A11). Acidification to pH 2.4 was done by using a 1 M HCl solution.

NMR Spectroscopy. NMR samples of uniformly ^{15}N labeled S100A11 were prepared with a monomer concentration of 108 μM in a 90% H_2O/10% D_2O mixture with 30 μM DSS as an internal standard. HSQC spectra (*38*) were collected on a Varian INOVA 600 MHz spectrometer using a pulsed-field gradient triple-resonance probe. Data were processed using NMRPipe (*39*) and analyzed using NMRView (*40*).

Time-Resolved ESI-MS. The details of the continuous-flow technique used for this study have been described elsewhere (*27*). Briefly, two syringes (termed 1 and 2) are connected to a concentric capillary mixing setup which is directly interfaced to a customized ESI source. Mixing of solutions from syringe 1 (120 μM monomeric S100A11 in dilute acetic acid, 10 μL/min) and syringe 2 (aqueous ammonia solution, 10 μL/min) results in a pH jump from 2.4 to 8.5, an ammonium acetate concentration of 500 mM, and a monomeric protein concentration of 60 μM. The reaction time is determined by the distance between the mixing point and the ESI source. This distance can be controlled by a stepper motor-driven mechanism.

Mass spectra were recorded on a Micromass/Waters (Manchester, U.K.) LCT time-of-flight mass spectrometer at a capillary voltage of 5000 V. The instrument was operated by using elevated pressures in the ion sampling region, to facilitate the detection of noncovalent protein complexes (*41*, *42*). A source pressure of 6 mbar, with sample cone and extraction cone voltages of 60 and 6 V, respectively, was found to give optimal signal intensities for the dimer. All data were acquired using the MassLynx instrument software. Time-dependent ion intensity profiles of individual ionic signals were extracted from the total ion count profiles by integrating each peak along its half-width. Laminar-flow effects within the capillary mixer were treated as described in ref *43*. Data for a reaction time of 5 min were obtained after manual mixing of the reactant solutions.

For on-line pulsed HDX, a second mixing step was incorporated into the experimental protocol. Syringes 1 and 2 were operated by using the same solutions and flow rates as described above. After a variable refolding time, the reaction mixture was exposed to excess D_2O from a third syringe (pD 8.5, 500 mM ammonium acetate, 80 μL/min)

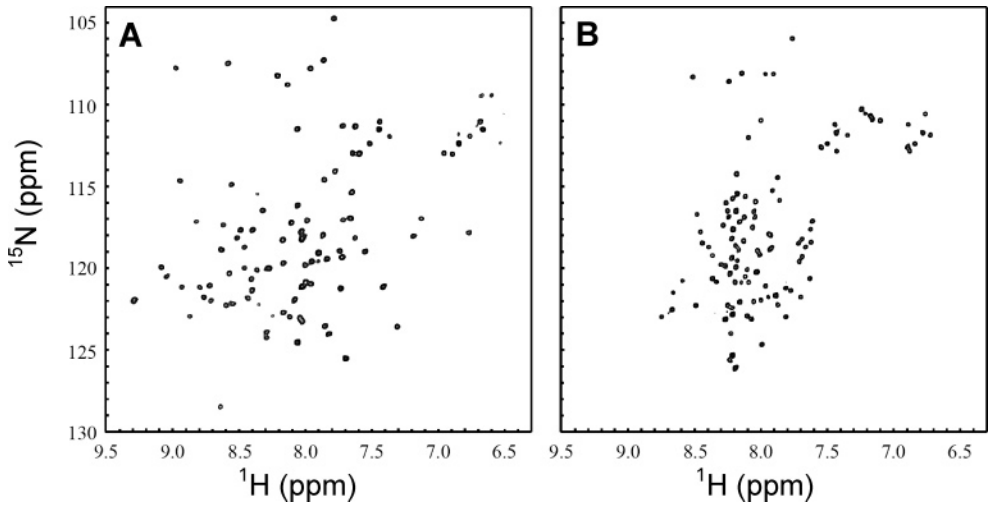

FIGURE 1: $^{1}H-^{15}N$ HSQC spectra of calcium-free S100A11 in a 90% H_2O/10% D_2O mixture. The native state spectrum (A) was collected at pH 7.3, and the spectrum of acid-denatured S100A11 (B) was collected at pH 2.4 using the same sample but with appropriate pH adjustments. Both spectra were acquired using identical NMR parameters.

for a total flow rate of 100 μL/min and a final protein concentration of 6 μM (based on dimeric protein). The isotope labeling pulse was terminated after 25 ms by solvent evaporation during ESI, which occurs on the time scale of 1 ms (*44*). The use of alkaline conditions for labeling is necessitated by the requirement for sufficiently large intrinsic HDX rate constants. At pD 8.5, the exchange of unprotected amide hydrogens occurs on a time scale of 10 ms (*45*, *46*). The use of a constant pH (or pD) throughout the double mixing sequence prevents potential artifacts associated with changes in the solution conditions during labeling (*47*). The quasi-instantaneous MS analysis after labeling used here allows the protein compactness (probed by the charge state distribution) to be directly correlated with the HDX behavior of the various coexisting conformers that become populated during the reaction. Consequently, two probes that simultaneously report on different aspects of the protein structure during folding are available (*27*, *48*). In addition, the progress of the protein assembly process is reflected in time-dependent changes of the monomer/dimer ratio in the ESI mass spectrum. The absence of a chemical quenching step implies that the measured HDX levels are due not only to amide groups but also to exchangeable sites on amino acid side chains and on the termini. For none of the refolding experiments was there any indication of protein aggregation.

RESULTS AND DISCUSSION

Acid-Denatured State of S100A11. Prior to studying the refolding of S100A11, we found it was instructive to explore the properties of the acid-denatured protein. Under native solvent conditions, both the amide proton chemical shift dispersion in the HSQC spectrum (Figure 1A) and the corresponding CD signature (Figure 2, dashed lines) are consistent with a highly ordered protein conformation. When the pH is lowered to 2.4, the protein adopts a more unfolded structure, as evidenced by the significantly diminished chemical shift dispersion and narrower ^{1}H line widths (Figure 1B) (*49*). In the CD spectrum, acid exposure leads to changes around 195 and 220 nm (Figure 2, solid lines), suggesting some alterations in the secondary structure of the protein (*50*). Specifically, the signal change at 222 nm indicates a

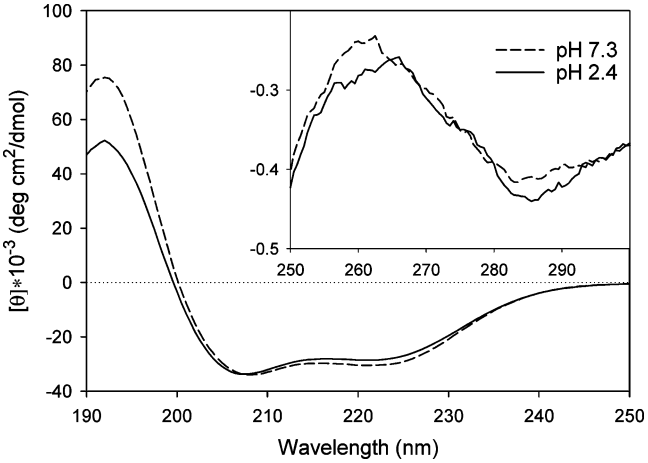

FIGURE 2: Far-UV and near-UV (inset) circular dichroism spectra of S100A11 recorded at pH 7.3 (− − −) and pH 2.4 (—). The data were recorded in the absence of calcium.

loss of α-helicity on the order of 6% (*51*). Spectral alterations in the 250−300 nm range are indicative of tertiary structural modifications in the local environment of aromatic amino acid side chains (S100A11 contains nine aromatics, Phe17, -35, -38, -46, -73, -76, -91, and -101 and Tyr20; there is no Trp) (*52*). Although these CD measurements confirm the occurrence of structural changes upon acid exposure, the degree of unfolding seems moderate when compared to data obtained for the denaturation of other proteins (*53*, *54*). Importantly, however, the ESI mass spectrum recorded at pH 2.4 exclusively shows monomeric ions (Figure 3A). This finding reveals that the protein does not maintain its intermolecular contacts under acidic conditions. The ESI charge state distribution is very wide and has a maximum around 12+. Comparison with ESI-MS data obtained for similarly sized proteins confirms that the spectrum in Figure 3A represents a non-native protein structure (*18*, *21*, *22*). This assertion is supported by comparing the spectrum in Figure 3A with that obtained for refolded S100A11 (discussed below; see Figure 3E). The observations made here confirm earlier reports (*55*) that suggested that the ESI charge state distribution can be more sensitive to conformational changes than CD spectroscopy. In conclusion, exposure of

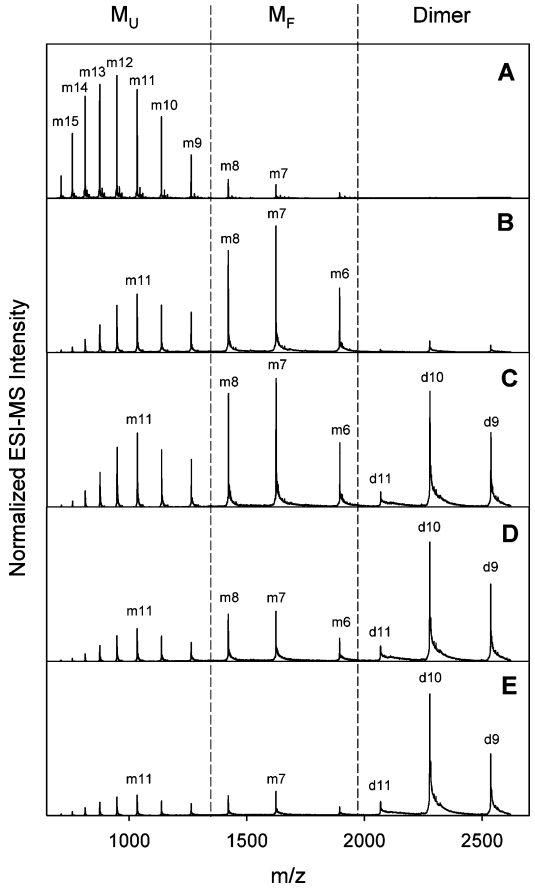

FIGURE 3: ESI mass spectra of S100A11 recorded in positive ion mode. (A) Acid-denatured protein in aqueous solution at pH 2.4. Time-resolved spectra, recorded 10 ms, 200 ms, 800 ms, and 5 min after a pH jump from 2.4 to 8.5, are shown in panels B−E, respectively. m11, m12, etc., represent charge states of monomeric protein ions (e.g., $[\text{monomer} + 12\text{H}]^{12+}$); d11, d10, and d9 represent dimeric protein ions (e.g., $[\text{dimer} + 10\text{H}]^{10+}$). Dashed lines separate the ionic signals attributed to three different kinetic species: M_U (unfolded monomer), M_F (folded monomer), and folded dimer.

calcium-free S100A11 to pH 2.4 causes disruption of the protein's dimeric structure. The resulting monomeric subunits adopt a moderately unfolded conformation, retaining a significant helicity, and some tertiary structural elements.

Refolding in the Absence of Calcium. Time-resolved ESI mass spectra recorded at different times after a pH jump to 8.5 allow tracking of the conformational changes associated with the formation of tightly folded apo-S100A11 homodimers, starting from acid-denatured monomers. For a reaction time of 10 ms (Figure 3B), the protein still is predominantly monomeric. Notably, the charge state distribution obtained under these conditions is bimodal, with maxima at +11 and +7. This observation indicates the presence of two distinct solution-phase conformations that differ in their overall compactness (*56*−*58*). Charge states around +11 are assigned to a more unfolded conformation, termed M_U. The charge state distribution of this species suggests that it has an overall compactness similar to that of the acid-denatured protein at pH 2.4 (Figure 3A). The slight shift in maximum from +12 to +11 may reflect a small conformational change. Alternatively, this effect could result from the different ionization conditions used (pH 2.4 vs pH 8.5), which might lead to a weakened charge acquisition during ESI under the conditions of Figure 3B (*27*). Charge

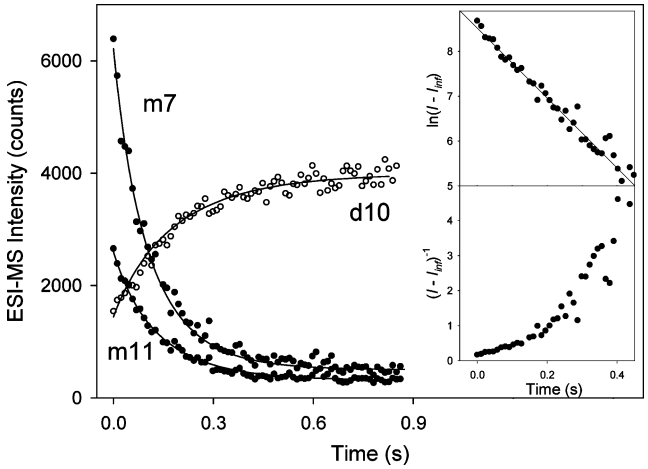

FIGURE 4: Intensity−time profiles for monomeric S100A11 in charge states +7 and +11 (●) and the dimeric protein in the +10 charge state (○). Solid lines are first-order fits to the experimental data, based on the deconvolution procedure outlined in ref *43*. Insets display first-order (top) and second-order (bottom) plots of the kinetic data obtained for the monomeric +7 charge state. I represents the measured count rate; the value of I_{inf} (=500 counts) was determined by averaging the intensities of the last 10 data points.

states around +7 in Figure 3B are assigned to monomeric proteins in a more tightly folded conformation, termed M_F. Panels C and D of Figure 3 show data recorded for reaction times of 200 and 800 ms, respectively. These spectra reveal increasing contributions of dimeric protein ions in charge states +9 to +11, whereas the relative intensities of the monomeric peaks steadily decrease. The final stage of the folding and assembly process is characterized by the data in Figure 3E, recorded 5 min after the pH jump. This spectrum is dominated by dimeric S100A11. The persistence of low-intensity monomeric signals is not surprising; for a K_d of 2 μM (*32*) at a total protein concentration of 60 μM (based on monomeric S100A11), the expected dimer/monomer ratio is 3.3/1. Spectra obtained for protein samples that had not been previously exposed to acidic conditions are indistinguishable from that depicted in Figure 3E (data not shown). Overall, the ESI-MS data of Figure 3 reveal that a pH jump from 2.4 to 8.5 causes S100A11 to undergo a transition from a denatured monomeric structure to a tightly folded dimer on a time scale of ∼1 s. This conversion is not a simple two-state process. Instead, it involves a monomeric kinetic intermediate, M_F, that is associated with charge states of around +7, which indicates a highly compact structure.

Intensity−time profiles of the ionic signals corresponding to M_F show decay kinetics similar to those of the charge states representing M_U (Figure 4). Although the overall kinetics for a monomer−dimer transition might be expected to show second-order behavior, this is not the case for the reaction studied here. Instead, apparent first-order kinetics are observed, as exemplified for the monomer +7 charge state (Figure 4, insets) (*59*). Accordingly, all of the monomer profiles were fitted by first-order expressions of the form $\exp(-k_{eff}t)$. The effective rate constant k_{eff} for the decay of M_F, determined as an average from fits of the monomeric +6 to +8 charge states, was found to be $6.9 \pm 0.5\ s^{-1}$. This value is similar to the average k_{eff} value of $6.0 \pm 0.5\ s^{-1}$ determined for M_U from fits of the +9 to +15 ionic signals. The formation of M_F occurs within the ∼10 ms dead time

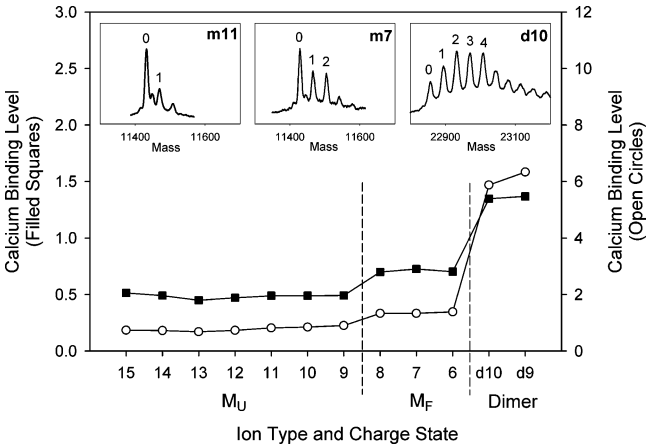

FIGURE 5: Calcium binding properties of monomeric and dimeric S100A11 ions in the ESI mass spectrum, measured 100 ms after the initiation of refolding. Final concentrations of Ca^{2+} and protein and were 100 and 10 μM (based on dimeric S100A11), respectively. Calcium binding levels were calculated in two different ways. Filled squares represent the intensity ratios of the single-calcium signal to the zero calcium peak. Empty circles represent data calculated in an analogous fashion but based on the sum of the one- and two-calcium peaks (for monomeric ions) and the sum of the one-, two-, three-, and four-calcium peaks (for dimeric ions). The insets show mass distributions for selected charge states. They were obtained by converting the *m*/*z* axis of the original data to mass *M* according to $M = i(m/z - 1)$, where *i* is the ion charge state ($i = 11$, 7, and 10 for m11, m7, and d10, respectively). The number of calcium ions corresponding to the individual peaks is indicated as zero, one, two, three, or four.

of the experiment such that an initial intensity rise that is often associated with the formation of a reaction intermediate is not observed in the corresponding intensity profiles. Also shown in Figure 4 are the formation kinetics of dimeric S100A11, exemplified by the +10 charge state. The rise of these dimeric signals is characterized by an average k_{eff} value of 5.0 ± 0.4 s^{-1}. The differences in the effective rate constants determined for M_F, M_U, and the dimer are likely due to limitations in the signal-to-noise ratio of the experimental data.

Refolding in the Presence of Calcium. The well-known interference of salts and other nonvolatile solvent additives with the ionization process makes ESI-MS studies at high calcium concentrations very difficult. As a consequence, it is common to carry out ESI-MS studies with calcium-binding proteins under nonsaturating conditions (*60*). S100A11 represents a particularly challenging case, since its calcium affinity is lower than that of many other S100 proteins (*33*). Using flow dialysis methods, Allen et al. (*61*) found that 10 mM Ca^{2+} was required to achieve saturation for protein concentrations comparable to those used here.

For this study, S100A11 refolding experiments analogous to those described above were carried at a final $CaCl_2$ concentration of 100 μM and a protein concentration of 10 μM after mixing (based on dimeric S100A11). The overall appearance of the charge state distributions and folding kinetics was found to be very similar to that of the data observed in the absence of calcium (see the previous section). However, the signal-to-noise ratio of the spectra obtained under these conditions was significantly compromised (data not shown). One very interesting aspect, however, is related to the calcium binding properties of the different species observed in the ESI mass spectrum (Figure 5). Monomeric signals attributed to M_U (+9 to +15) are dominated by calcium-free protein ions, with only minor satellite peaks corresponding to singly calciated species. In comparison, the monomer charge states of +6 to +8, which had been assigned to M_F, exhibit much stronger satellite peaks, reflecting ions bound to one and two calcium ions (Figure 5, insets). Within each of the two groups of charge states, the calcium binding level remains remarkably constant. The two monomeric conformations, M_U and M_F, that had initially been identified on the basis of their charge state distributions, therefore, show very distinct metal binding properties. M_F, which corresponds to a more tightly folded structure, exhibits a higher Ca^{2+} affinity than M_U. Dimerization of S100A11 results in another marked increase in calcium binding affinity. The mass distributions of the dimeric protein exhibit maximum intensity levels for complexes containing two to four calcium ions. The calcium binding levels observed for the various protein ions remain virtually unchanged for all the time points that have been studied (data not shown).

Close inspection of the mass distributions in Figure 5 reveals the presence of additional signals corresponding to monomeric S100A11 bound to more than two and dimeric ions carrying more than four calcium ions. These metal loading levels are higher than those expected on the basis of the known number of binding sites in the protein. These signals are attributed to nonspecific metal−protein complexes generated during the ESI process. Complexation events of this type are very common when protein solutions containing nonvolatile cations are electrosprayed (*62*, *63*). Nonetheless, it appears that the calcium distributions of Figure 5 are predominantly governed by specific binding events. This assertion is supported by the fact that the calcium binding behavior is strongly correlated with the type of protein species (M_U, M_F, and dimer). In addition, there are clear discontinuities within the intensity progressions of the individual calcium peaks; e.g., the excess calcium peaks for monomeric +7 ions are much weaker than the signals of singly and doubly loaded S100A11. Similarly, there is a clear discontinuity between the fourth and fifth calcium for the dimeric protein (see the insets of Figure 5).

Time-Resolved ESI with On-Line Pulsed HDX. In an attempt to uncover additional information about the S100A11 refolding mechanism, a pulsed isotope labeling step was incorporated into the experimental protocol. The measurements were conducted without calcium, to maintain an acceptable signal-to-noise ratio. Pulse labeling of the protein for 25 ms immediately prior to ionization results in peak splitting for all the monomer charge states (Figure 6A−D and Figure 6E−H). The two major maxima exhibited by the resulting mass distributions correspond to shifts of ca. 110 and 140 Da. For all monomer signals, the relative intensity of the high-mass portion decreases, whereas that of the low-mass peak increases as the reaction proceeds. The charge states assigned to M_U (+9 to +15) exhibit a behavior similar to those representing M_F (+6 to +8), although the high-mass portion is somewhat more pronounced for the latter throughout the entire time range that was studied. No such splitting was observed for dimeric S100A11 (Figure 6I−L). The mass shift around 220 Da exhibited by the dimer is indistinguishable from the that of the low-mass monomeric peak (110 Da), when considered on a per-subunit basis. The measured shifts are charge state-independent, and they remain

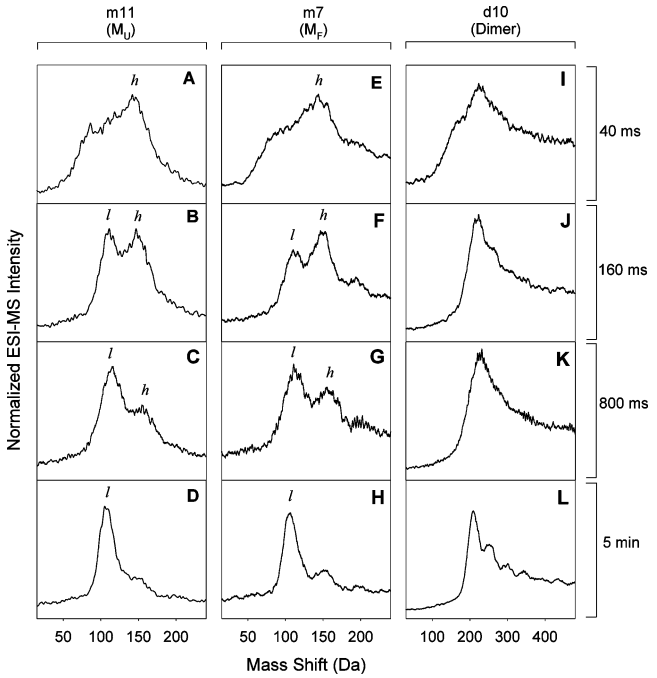

FIGURE 6: Mass distributions obtained after pulse labeling of S100A11 during refolding for different time points: (A−D) +11 monomer, (E−H) +7 monomer, and (I−L) +10 dimer. In the top row (A, E, and I), reaction time $t = 40$ ms. In the second row (B, F, and J), $t = 160$ ms. In the third row (C, G, and K), $t = 800$ ms. In the bottom row (D, H, and L), $t = 5$ min. The *x*-axes display the mass shift, ΔM, relative to unlabeled S100A11. Mass shift values were obtained by converting the *m*/*z* axis of the original data according to $\Delta M = m/z \times i - 0.8M_D i - 0.2M_H i - M_0$, where M_0 is the mass of the unlabeled protein (monomer or dimer), i is the ion charge state, and M_D and M_H are the masses of deuterium (2.014 Da) and protium (1.008 Da), respectively. The resulting mass shift values were divided by 0.8 to take into account the isotopic composition of the labeling solution. Labels "*l*" and "*h*" indicate the low-mass and high-mass components, respectively, of monomeric split peaks in panels A−H. Minimal smoothing was applied to the original data, using the MassLynx instrument software.

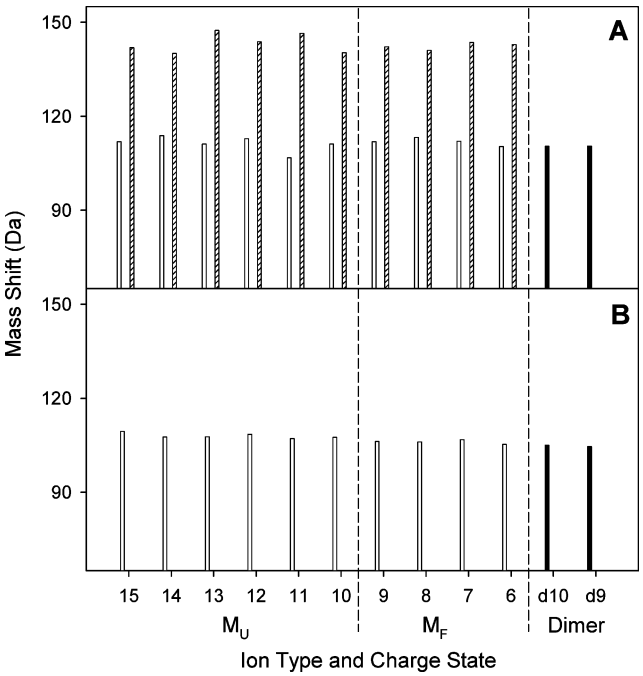

FIGURE 7: Mass shifts after pulsed HDX, determined from the peak maxima of monomeric and dimeric ions for reaction times of 100 ms (A) and 5 min (B). Dimer mass shifts have been divided by a factor of 2, to allow a direct comparison to data obtained for monomeric species. The two values shown in panel A for each of the monomer states are derived from the two maxima of the corresponding bimodal mass distributions (see Figure 6).

almost unchanged for the entire experimental time window of 5 min (Figure 7).

The observed peak splitting reveals that M_U and M_F are each comprised of two subspecies that exhibit different HDX characteristics. Thus, a total of four distinct monomeric forms of S100A11 can be distinguished. The two conformers with high exchange levels will be termed M_U^h and M_F^h, whereas the less extensively labeled species are designated M_U^l and M_F^l. The mass shift of ~140 Da measured for M_U^h and M_F^h corresponds to a relative exchange level of 77%. In comparison, the mass shifts observed for M_U^l and M_F^l represent an exchange level of only 60%. According to the time-dependent changes in the intensity ratio of high-mass versus low-mass peaks in Figure 6, the population of monomeric S100A11 shortly after mixing is dominated by M_U^h and M_F^h. As the reaction proceeds, the relative contributions of the less extensively labeled monomers (M_U^l and M_F^l) steadily increase. It is interesting that the transitions from M_U^h to M_U^l, and from M_F^h to M_F^l, are not accompanied by notable shifts in the corresponding ESI charge state distributions (Figure 3). This suggests that the two M_U species exhibit conformations that are extended to a similar degree. Analogously, the two M_F species appear to share structures that are similar to each other, but more compact. As discussed earlier (Figure 5), the calcium binding properties of M_U and M_F do not depend on the reaction time. This implies that the structural differences of M_U^h versus M_U^l (and M_F^h versus M_F^l) do not significantly affect the EF-hand calcium binding regions of the protein.

The width of a protein mass distribution after pulsed HDX provides information about the heterogeneity of the solution-phase conformation with respect to its exchange accessibility. Heterogeneous populations of proteins will exhibit wider distributions than structurally uniform conformers (*45*, *64*). The mass distributions measured for all the S100A11 ionic species after pulsed labeling show a notable reduction in their overall peak width with increasing reaction times. This is most apparent when comparing the top row of Figure 6, representing a reaction time of 40 ms (panels A, E, and I), with the data obtained for 5 min (panels D, H, and L). This peak narrowing implies that each of the kinetic species involved in the refolding of S100A11 exhibits a significant degree of conformational heterogeneity for early times. As the reaction proceeds, the individual species become structurally more homogeneous. These observations made here for S100A11 are consistent with "structural fine-tuning" processes observed earlier during the reconstitution of holomyoglobin (*28*).

Mechanism of S100A11 Folding and Dimerization. On the basis of the time-resolved data presented in this work, an overall model for the refolding and assembly of S100A11 can be proposed (Figure 8). Protein conformers that undergo rapid interconversion during the 25 ms isotope labeling pulse will exhibit indistinguishable HDX properties, regardless of possible differences in their structure (*65*). The observation of two distinct labeling levels for the various kinetic species, therefore, suggests the existence of two pools of rapidly interconverting conformers, as indicated by the boxes in

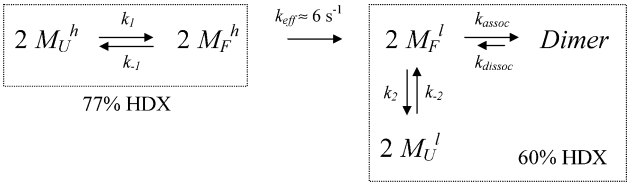

FIGURE 8: Possible kinetic model for the refolding and dimerization of S100A11. The notation used is explained in the text. Species grouped together in boxes are in rapid equilibrium with each other. Also indicated are the measured HDX levels observed after pulsed isotope labeling.

Figure 8. The first of these pools comprises monomers M_U^h and M_F^h, which exhibit an exchange level of 77%. Analogously, rapid interconversion takes place among M_U^l, M_F^l, and dimeric S100A11 (60% exchange level). For the species within each of these two pools to be indistinguishable by pulsed HDX, the first-order rate constants k_1, k_{-1}, k_2, and k_{-2} have to be significantly larger than $(25\ ms)^{-1} = 40\ s^{-1}$. This also holds for the dissociation rate constant k_{dissoc}. From this estimate of k_{dissoc} and on the basis of a K_d or k_{dissoc}/k_{assoc} value of 2 μM (*32*), it follows that the association rate constant k_{assoc} should be considerably greater than $2 \times 10^7\ M^{-1}\ s^{-1}$. Although this value is larger than the corresponding rate constants for many other complexes, the estimate does not seem unreasonable, considering that k_{assoc} values approaching the diffusion limit of $10^9\ M^{-1}\ s^{-1}$ have previously been reported for a number of systems (*16*, *66*, *67*).

The first-order nature of the measured kinetics (with $k_{eff} \approx 6\ s^{-1}$; Figure 4) implies that the rate-determining step of the overall reaction is a unimolecular event, i.e., a process occurring at the monomer level (*16*). Unfortunately, the rapid equilibration processes discussed above preclude an unambiguous arrangement of the various species within a kinetic mechanism (*68*). As a result, it cannot be determined with certainty which of the two species, M_U^h or M_F^h, undergoes the rate-determining step. Similarly, it is not possible to pinpoint whether M_U^l or M_F^l, or possibly an additional weakly populated intermediate, is the primary product of this transition. Consequently, the arrangement proposed in Figure 8 is only one of several possibilities that are consistent with the observed kinetics. It has M_U^h as the starting point of the S100A11 folding mechanism, representing an extended and relatively disordered structure. Collapse of this species generates a more compact conformation, M_F^h, within the dead time of the experiment. The next step is a slow transition leading to M_F^l, which can rapidly assemble into the dimeric, native structure. In this proposed scenario, M_U^l is considered to be an off-pathway intermediate (*69*). The mechanism depicted in Figure 8 was chosen because it highlights the possible existence of a linear folding pathway, with a sequence of increasingly nativelike structures en route to the native state. Such a scenario resembles the folding mechanisms of many single-chain proteins (*70*−*74*). Analogous progressions, involving tightly folded monomers as transient intermediates, are thought to be operational during the formation of other multiprotein complexes (*6*−*13*, *16*).

CONCLUSIONS

This work clearly illustrates the utility of time-resolved ESI-MS with on-line HDX for mechanistic studies on rapid assembly processes, leading from denatured monomeric subunits to multiprotein complexes. Classical HDX experiments employing quench-flow strategies with subsequent off-line MS or NMR analysis of the labeled protein would have revealed the presence of merely two kinetic species, namely, proteins exhibiting "high" and "low" labeling levels (*64*, *75*). Conversely, an analysis based solely on time-resolved ESI mass spectra would have uncovered only three distinct species, namely, two monomer conformations exhibiting a different overall compactness (M_U and M_F) in addition to dimeric S100A11. This work, however, combines the two approaches such that time-resolved ESI mass spectra and the protein HDX behavior can be monitored simultaneously as nonredundant probes of protein structure in solution. As a result, four distinct monomeric species can be identified that are involved in the folding and assembly of acid-denatured S100A11. The proposed overall mechanism is consistent with folding−assembly processes observed for other protein complexes, in that it involves a progression from denatured to increasingly nativelike monomers, followed by quaternary structure formation (*6*−*13*, *16*). It would be interesting to carry out refolding experiments analogous to those described here by employing a much shorter pulse labeling step. In principle, this should allow a differentiation of the various conformers within the two pools of species, as well as a direct visualization of conformational interconversion events within these pools (*48*). Unfortunately, the current setup precludes the use of much shorter labeling times. Efforts to implement novel mixer designs for ultrarapid HDX studies are currently being explored in our laboratory.

ACKNOWLEDGMENT

We thank Derek J. Wilson for helpful discussions.

REFERENCES

1. Anfinsen, C. B. (1973) Principles that Govern the Folding of Protein Chains, *Science 181*, 223−230.
2. Baker, D. (2000) A surprising simplicity to protein folding, *Nature 405*, 39−42.
3. Daggett, V., and Fersht, A. (2003) The present view of the mechanism of protein folding, *Nat. Rev. Mol. Cell Biol. 4*, 497−502.
4. Rumbley, J., Hoang, L., Mayne, L., and Englander, S. W. (2001) An amino acid code for protein folding, *Proc. Natl. Acad. Sci. U.S.A. 98*, 105−112.
5. Onuchic, J. N., and Wolynes, P. G. (2004) Theory of protein folding, *Curr. Opin. Struct. Biol. 14*, 70−75.
6. Mann, C. J., and Matthews, C. R. (1993) Structure and Stability of an Early Folding Intermediate of *Escherichia coli* trp Aporepressor Measurerd by Far-UV Stopped-Flow Circular Dichroism and 8-Anilino-1-naphthalene Sulfonate Binding, *Biochemistry 32*, 5282−5290.
7. Jaenicke, R. (1991) Protein Folding: Local Structures, Domains, Subunits, and Assemblies, *Biochemistry 30*, 3147−3161.
8. Minton, A. P. (2000) Implications of macromolecular crowding for protein assembly, *Curr. Opin. Struct. Biol. 10*, 34−39.
9. Nichtl, A., Buchner, J., Jaenicke, R., Rudolph, R., and Scheibl, T. (1998) Folding and Association of β-Galactosidase, *J. Mol. Biol. 282*, 1083−1091.
10. Mateu, M. G., Pino, M. M. S. D., and Fersht, A. R. (1999) Mechansim of folding and assembly of a small tetrameric protein domain from tumor suppressor p53, *Nat. Struct. Biol. 6*, 191−198.
11. Shakhnovich, E. I. (1999) Folding by association, *Nat. Struct. Biol. 6*, 99−102.
12. Verkhivker, G. M., Bouzida, D., Gehlhaar, D. K., Rejto, P. A., Freer, S. T., and Rose, P. W. (2003) Simulating disorder−order

transition in molecular recognition of unstructured proteins: Where folding meets binding, *Proc. Natl. Acad. Sci. U.S.A. 100*, 5148−5153.
13. Gunasekaran, K., Tsai, C.-J., Kumar, S., Zanuy, D., and Nussinov, R. (2003) Extended disordered proteins: Targeting function with less scaffold, *Trends Biochem. Sci. 28*, 81−85.
14. Shoemaker, B. A., Portman, J. J., and Wolynes, P. G. (2000) Speeding molecular recognition by using the folding funnel: The fly-casting mechanism, *Proc. Natl. Acad. Sci. U.S.A. 97*, 8868−8873.
15. Crespin, M. O., Boys, B. L., and Konermann, L. (2005) The reconstitution of unfolded myoglobin with hemin dicyanide is not accelerated by fly casting, *FEBS Lett. 579*, 271−274.
16. Seckler, R. (2000) in *Mechanisms of Protein Folding* (Pain, R. H., Ed.) Oxford University Press, Oxford, U.K.
17. Fändrich, M., Tito, M. A., Leroux, M. R., Rostom, A. A., Hartl, F. U., Dobson, C. M., and Robinson, C. V. (2000) Observation of the noncovalent assembly and disassembly pathways of the chaperone complex MtGimC by mass spectrometry, *Proc. Natl. Acad. Sci. U.S.A. 97*, 14151−14155.
18. Kaltashov, I. A., and Eyles, S. J. (2002) Studies of Biomolecular Conformations and Conformational Dynamics by Mass Spectrometry, *Mass Spectrom. Rev. 21*, 37−71.
19. Kaltashov, I. A., and Eyles, S. J. (2005) *Mass Spectrometry in Biophysics*, John Wiley and Sons, Inc., Hoboken, NJ.
20. Heck, A. J. R., and Van den Heuvel, R. H. H. (2004) Investigation of intact protein complexes by mass spectrometry, *Mass Spectrom. Rev. 23*, 368−389.
21. Chowdhury, S. K., Katta, V., and Chait, B. T. (1990) Probing Conformational Changes in Proteins by Mass Spectrometry, *J. Am. Chem. Soc. 112*, 9012−9013.
22. Grandori, R., Matecko, I., and Muller, N. (2002) Uncoupled analysis of secondary and tertiary protein structure by circular dichroism and electrospray ionization mass spectrometry, *J. Mass Spectrom. 37*, 191−196.
23. Nemirovskiy, O. V., Ramanathan, R., and Gross, M. L. (1997) Investigation of Calcium-Induced, Noncovalent Association of Calmodulin with Melittin by Electrospray Ionization Mass Spectrometry, *J. Am. Soc. Mass Spectrom. 8*, 809−812.
24. Vis, H., Heinemann, U., Dobson, C. M., and Robinson, C. V. (1998) Detection of a Monomeric Intermediate Associated with Dimerization of Protein Hu by Mass Spectrometry, *J. Am. Chem. Soc. 120*, 6427−6428.
25. Simmons, D. A., Wilson, D. J., Lajoie, G. A., Doherty-Kirby, A., and Konermann, L. (2004) Subunit Disassembly and Unfolding Kinetics of Hemoglobin Studied by Time-resolved Electrospray Mass Spectrometry, *Biochemistry 43*, 14792−14801.
26. Wilson, D. J., Rafferty, S. P., and Konermann, L. (2005) Kinetic Unfolding Mechanism of the Inducible Nitric Oxide Synthase Oxygenase Domain Determined by Time-Resolved Electrospray Mass Spectrometry, *Biochemistry 44*, 2276−2283.
27. Pan, J. X., Wilson, D. J., and Konermann, L. (2005) Pulsed Hydrogen Exchange and Electrospray Charge-State Distribution as Complementary Probes of Protein Structure in Kinetic Experiments: Implications for Ubiquitin Folding, *Biochemistry 44*, 8627−8633.
28. Simmons, D. A., and Konermann, L. (2002) Characterization of Transient Protein Folding Intermediates During Myoglobin Reconstitution by Time-Resolved Electrospray Mass Spectrometry with On-Line Isotopic Pulse Labeling, *Biochemistry 41*, 1906−1914.
29. Schaefer, B. W., and Heizmann, C. W. (1996) The S100 family of EF-hand calcium-binding proteins: Functions and pathology, *Trends Biochem. Sci. 21*, 134−140.
30. Rety, S., Osterloh, D., Arie, J.-P., Tabaries, S., Seeman, J., Russo-Marie, F., Gerke, V., and Lewit-Bentley, A. (2000) Structural basis of the Ca^{2+}-dependent association between S100C (S100A11) and its target, the N-terminal part of annexin I, *Structure 8*, 175−184.
31. Fernandez-Fernandez, M. R., Veprintsev, D. B., and Fersht, A. R. (2005) Protein of the S100 family regulate the oligomerization of p53 tumor suppressor, *Proc. Natl. Acad. Sci. U.S.A. 102*, 4735−4740.
32. Wang, G., Zhang, S. G., Fernig, D. G., Spiller, D., Martin-Fernandez, M., Zhang, H., Ding, Y., Rudland, P. S., and Barraclough, R. (2004) Heterodimeric interaction and interfaces of S100A1 and S100P, *Biochem. J. 382*, 375−383.
33. Dempsey, A. C., Walsh, M. P., and Shaw, G. S. (2003) Unmasking the annexin I interaction from the structure of apo-S100A11, *Structure 11*, 887−897.
34. Murakami, K., Yumoto, F., Ohki, S.-Y., Yasunaga, T., Tanokura, M., and Wakabayashi, T. (2005) Structural Basis for Ca^{2+}-regulated Muscle Relaxation at Interaction Sites of Troponin with Actin and Tropomyosin, *J. Mol. Biol. 352*, 178−201.
35. Heidorn, D. B., Seeger, P. A., Rokop, S. E., Blumenthal, D. K., Means, A. R., Crespi, H., and Trewhella, J. (1989) Changes in the Structure of Calmodulin Induced by a Peptide Based on the Calmodulin-Binding Domain of Myosin Light Chain Kinase, *Biochemistry 28*, 6757−6764.
36. Glasoe, P. K., and Long, F. A. (1960) Use of glass electrodes to measure acidities in deuterium oxide, *J. Phys. Chem. 64*, 188−190.
37. Rintala, A. C., Schöekess, B. O., Walsh, M. P., and Shaw, G. S. (2002) Letter to the Editor: ^{1}H, ^{15}N and ^{13}C resonance assignments of rabbit apo-S100A11, *J. Biomol. NMR 22*, 191−192.
38. Kay, L. E., Keifer, P., and Saarinen, T. (1992) Pure absorption gradient enhanced heteronuclear single quantum correlation spectroscopy with improved sensitivity, *J. Am. Chem. Soc. 114*, 10663−10665.
39. Delaglio, F., Grzesiek, S., Vuister, G. W., Zhu, G., Pfeifer, J., and Bax, A. (1995) NMRPipe: A multidimensional spectral processing system based on UNIX pipes, *J. Biomol. NMR 6*, 277−293.
40. Johnson, B. A., and Belvins, R. A. (1994) NMRView: A computer program for the visualization and analysis of NMR data, *J. Biomol. NMR 4*, 603−614.
41. Tahallah, N., Pinkse, M., Maier, C. S., and Heck, A. J. R. (2001) The effect of the source pressure on the abundance of ions of noncovalent protein assemblies in an electrospray ionization orthogonal time-of-flight instrument, *Rapid Commun. Mass Spectrom. 15*, 596−601.
42. Chernushevich, I. V., and Thomson, B. A. (2004) Collisional cooling of large ions in electrospray mass spectrometry, *Anal. Chem. 76*, 1754−1760.
43. Wilson, D. J., and Konermann, L. (2003) A Capillary Mixer with Adjustable Reaction Chamber Volume for Millisecond Time-Resolved Studies by Electrospray Mass Spectrometry, *Anal. Chem. 75*, 6408−6414.
44. Kebarle, P., and Tang, L. (1993) From ions in solution to ions in the gas phase: The mechanism of electrospray mass spectrometry, *Anal. Chem. 65*, 972−986.
45. Konermann, L., and Simmons, D. A. (2003) Protein Folding Kinetics and Mechanisms Studied by Pulse-Labeling and Mass Spectrometry, *Mass Spectrom. Rev. 22*, 1−26.
46. Bai, Y., Milne, J. S., Mayne, L., and Englander, S. W. (1993) Primary Structure Effects on Peptide Group Hydrogen Exchange, *Proteins: Struct., Funct., Genet. 17*, 75−86.
47. Bieri, O., and Kiefhaber, T. (2001) Origin of Apparent Fast and Non-exponential Kinetics of Lysozyme Folding Measured in Pulsed Hydrogen Exchange Experiments, *J. Mol. Biol. 310*, 919−935.
48. Simmons, D. A., Dunn, S. D., and Konermann, L. (2003) Conformational Dynamics of Partially Denatured Myoglobin Studied by Time-Resolved Electrospray Mass Spectrometry With Online Hydrogen−Deuterium Exchange, *Biochemistry 42*, 5896−5905.
49. Chatterjee, A., Kumar, A., Chugh, J., Srivastava, S., Bhavesh, N. S., and Hosur, R. V. (2005) NMR of unfolded proteins, *J. Chem. Sci. 117*, 3−21.
50. Greenfield, N., and Fasman, G. D. (1969) Computed Circular Dichroism Spectra for the Evaluation of Protein Conformation, *Biochemistry 8*, 4108−4116.
51. Chen, Y., Yang, J. T., and Martinez, H. M. (1972) Determination of the Secondary Structure of Proteins by Circular Dichroism and Optical Rotatory Dispersion, *Biochemistry 11*, 4120−4131.
52. Bychkova, V. E., Dujsekina, A. E., Klenin, S. I., Tiktopulo, E. I., Uversky, V. N., and Ptitsyn, O. B. (1996) Molten Globule-Like State of Cytochrome *c* under Conditions Simulating Those Near the Membrane Surface, *Biochemistry 35*, 6058−6063.
53. Griffith, W. P., and Kaltashov, I. A. (2003) Highly asymmetric interactions between globin chains during hemoglobin assembly revealed by electrospray ionization mass spectrometry, *Biochemistry 42*, 10024−10033.
54. Konermann, L., and Douglas, D. J. (1997) Acid-Induced Unfolding of Cytochrome *c* at Different Methanol Concentrations: Electro-

spray Ionization Mass Spectrometry Specifically Monitors Changes in the Tertiary Structure, *Biochemistry 36*, 12296−12302.
55. Pan, X. M., Sheng, X. R., and Zhou, J. M. (1997) Probing subtle acid-induced conformational changes of ribonuclease A by electrospray mass spectrometry, *FEBS Lett. 402*, 25−27.
56. Grandori, R. (2002) Detecting equilibrium cytochrome *c* folding intermediates by electrospray ionization mass spectrometry: Two partially folded forms populate the molten globule state, *Protein Sci. 11*, 453−458.
57. Dobo, A., and Kaltashov, I. A. (2001) Detection of Multiple Protein Conformational Ensembles in Solution via Deconvolution of Charge-State Distributions in ESI MS, *Anal. Chem. 73*, 4763−4773.
58. Mohimen, A., Dobo, A., Hoerner, J. K., and Kaltashov, I. A. (2003) A Chemometric Approach to Detection and Characterization of Multiple Protein Conformers in Solution Using Electrospray Ionization Mass Spectrometry, *Anal. Chem. 75*, 4139−4147.
59. Adams, P. A. (1977) The Kinetics of the Recombination Reaction between Apomyoglobin and Alkaline Haematin, *Biochem. J. 163*, 153−158.
60. Hill, T. J., Lafitte, D., Wallace, J. I., Cooper, H. J., Tsvetkov, P. O., and Derrick, P. J. (2000) Calmodulin-Peptide Interactions: Apocalmodulin Binding to the Myosin Light Chain Kinase Target Site, *Biochemistry 39*, 7284−7290.
61. Allen, B. G., Durussel, I., Walsh, M. P., and Cox, J. A. (1996) Characterization of the Ca^{2+}-binding properties of calgizzarin (S100C) isolated from chicken gizzard smooth muscle, *Biochem. Cell Biol. 74*, 687−694.
62. Hu, P., Ye, Q.-Z., and Loo, J. A. (1994) Calcium Stoicheometry Determination for Calcium Binding Proteins by Electrospray Ionization Mass Spectrometry, *Anal. Chem. 66*, 4190−4194.
63. Verkerk, U. H., and Kebarle, P. (2005) Ion−Ion and Ion−Molecule Reactions at the Surface of Proteins Produced by Nanospray. Information on the Number of Acidic Residues and Control of the Number of Ionized Acidic and Basic Residues, *J. Am. Soc. Mass Spectrom. 16*, 1325−1341.
64. Tsui, V., Garcia, C., Cavagnero, S., Siuzdak, G., Dyson, H. J., and Wright, P. E. (1999) Quench-flow experiments combined with mass spectrometry show apomyoglobin folds through an obligatory intermediate, *Protein Sci. 8*, 45−49.
65. Wagner, D. S., and Anderegg, R. J. (1994) Conformation of Cytochrome *c* Studied by Deuterium Exchange-Electrospray Ionization Mass Spectrometry, *Anal. Chem. 66*, 706−711.
66. Northrup, S. H., and Erickson, H. P. (1992) Kinetics of protein−protein association explained by Brownian dynamics computer simulations, *Proc. Natl. Acad. Sci. U.S.A. 89*, 3338−3342.
67. Baldwin, R. L. (1996) Why is protein folding so fast? *Proc. Natl. Acad. Sci. U.S.A. 93*, 2627−2628.
68. Fersht, A. R. (1999) *Structure and Mechanism in Protein Science*, W. H. Freeman & Co., New York.
69. Laurents, D. V., Bruix, M., and Jamin, B. R. L. (1998) A Pulse-Chase-Competition Experiment to Determine if a Folding Intermediate is On or Off-pathway: Application to Ribonuclease A, *J. Mol. Biol. 283*, 669−678.
70. Maity, H., Maity, M., and Englander, S. W. (2004) How Cytochrome *c* Folds, and Why: Submolecular Foldon Units and their Stepwise Sequential Stabilization, *J. Mol. Biol. 343*, 223−233.
71. Baldwin, R. L., and Rose, G. D. (1999) Is protein folding hierarchic? I. Local structure and peptide folding, *Trends Biol. Sci. 24*, 26−33.
72. Baldwin, R. L., and Rose, G. D. (1999) Is protein folding hierarchic? II. Folding intermediates and transition states, *Trends Biol. Sci. 24*, 77−83.
73. Bachmann, A., and Kiefhaber, T. (2001) Apparent Two-state Tendamistat Folding is a Sequential Process Along a Defined Route, *J. Mol. Biol. 306*, 375−386.
74. Weinkam, P., Zong, C., and Wolynes, P. G. (2005) A funneled energy landscape for cytochrome *c* directly predicts the sequential folding route inferred from hydrogen exchange experiments, *Proc. Natl. Acad. Sci. U.S.A. 102*, 12401−12406.
75. Heidary, D. K., Gross, L. A., Roy, M., and Jennings, P. A. (1997) Evidence for an obligatory intermediate in the folding of Interleukin-1β, *Nat. Struct. Biol. 4*, 725−731.

BI052349A